Fluid Age-based Analysis of a Lifted Turbulent DME Jet Flame DNS

Dong-Hyuk Shin[1], Edward S. Richardson[2], Vlad Aparace-Scutariu[1], Yuki Minamoto[3], and Jacqueline H. Chen[4]

[1] The School of Engineering, University of Edinburgh, Edinburgh, EH9 3DW, United Kingdom
[2] The Faculty of Engineering and the Environment, University of Southampton, Southampton, SO17 1BJ, United Kingdom
[3] Tokyo Institute of Technology, Meguro, Tokyo 152-8550, Japan
[4] Combustion Research Facility, Sandia National Laboratories, Livermore, CA 94550, USA

Abstract

The link between the distribution of fluid residence time and the distribution of reactive scalars is analysed using Direct Numerical Simulation data. Information about the reactive scalar distribution is needed in order to model the reaction terms that appear in Large Eddy and Reynolds-Averaged simulations of turbulent reacting flows. The lifted flame is simulated taking account of multi-step chemistry for dimethyl-ether fuel. Due to autoignition and flame propagation, the reaction progress increases with residence time. The variation of fluid residence time is evaluated by solving an Eulerian transport equation for the fluid age. The fluid age is a passive scalar with a spatially-uniform source term, meaning that its moments and dissipation rates in turbulent flows can be modelled using closures already established for conserved scalars such as mixture fraction. In combination with the mixture fraction, the fluid age serves as a useful mapping variable to distinguish younger less-reacted fluid near the inlet from older more-reacted fluid downstream. The local fluctuations of mixture fraction and fluid age have strong negative correlation and, building upon established presumed-pdf models for mixture fraction, this feature can be used to construct an accurate presumed-pdf model for the joint mixture fraction/fluid age pdf. It is demonstrated that the double-conditional first-order moment closure combined with the proposed presumed model for the joint pdf of mixture fraction and fluid age gives accurate predictions for unconditional reaction rates – both for pre-ignition radical species produced by low-temperature processes upstream of the flame base, and for major species that are produced at the flame front.

Keywords (max 5)

turbulence, autoignition, presumed pdf, residence time, age

1. Introduction

The residence time distribution is used widely in the process industry as a basis for modelling the progress of kinetically-limited processes within a given system. In combustion modelling, the residence time or *age* of fluid at different points within a flow has been used to estimate when and where a mixture will reach its ignition delay time and autoignite [1,2], or to track the relatively slow accumulation or burn out of pollutant species within the products of a flame [3,4]. The fluid age is defined as a spatially and temporally-varying continuum property of the fluid, equal to the mass-weighted average time that the atoms at each point have been within a specified domain [5]. The fluid age distribution within a combustion system may provide information useful for turbulent combustion modelling in two main ways. First, it can be used to measure how long particular reactants have been in contact and, if they have sufficient energy to react, this may be related to the progress of their reaction [6-8], subject to the additional influence of unsteady turbulent mixing [9]. Second, even if the reactants enter the domain with insufficient thermal energy to start reacting, the fluid age varies across the combustion chamber and provides a scalar marker field that can be used more generally as a basis for characterising turbulent mixing within any flames that occur inside a combustion chamber [10].

Despite the long-standing use of residence time distributions in process engineering, little is known about the local distribution of fluid age within turbulent combustion systems, or how the distribution of fluid age might be related to the local distribution of reactive scalars. Due to the difficulty of tracking the residence time of individual atoms in turbulent combustion experiments, evaluation of the local fluid age distributions within a turbulent flow relies upon direct numerical simulation (DNS). Assuming equal species diffusivities $\mathscr{D}$, the transport equation for fluid age a is given by [5,11,12],

$$\frac{\partial a}{\partial t} + \vec{u} \cdot \nabla a = \frac{1}{\rho} \nabla \cdot \left(\rho \mathscr{D} \nabla a \right) + 1, \tag{1}$$

where $\vec{u}$ is the velocity vector and ρ is the fluid density. The source term on the right hand side of Eq. (1) is equal to unity, representing the increase of age due to the passage of time. Conventionally the fluid age is set equal to zero at entry to the system, however the absolute value of fluid age is arbitrary, and Bilger [10] and Grout [4] use age as a marker field with its datum point at the flame surface. Equation (1) can be solved in DNS of turbulent flow in order to provide the distribution of fluid age throughout the flow [5], or used to derive moment equations for Reynolds-averaged or Large Eddy Simulations [1]. Since the source term in Eq. (1) is spatially-uniform, the source term does not contribute to gradient generation within the free-stream of the flow and the fluid age therefore mixes in a manner similar to a conserved scalar, such as mixture fraction, for which algebraic and transport equation modelling is well-established.

Shin *et al.* used DNS to investigate the distribution of the jet fluid age in statistically-stationary [5] and decelerating [13] turbulent round jets. In both cases, moments of the jet fluid age exhibit self-similar profiles downstream of an initial development region. Figure 1 shows the iso-lines of the mean mixture fraction and the mean mass-weighted jet fluid age for the statistically-stationary round jet [5]. The mean age of the jet fluid increases along the centreline of the jet, while the centreline mean mixture fraction decreases in inverse proportion to the stream-wise position. The self-similar profiles for the jet fluid age also differ from those for mixture fraction. The independent variation of the mean mixture fraction and mean jet fluid age leads to a unique mapping between the axial-radial coordinates of physical space, and the two-dimensional space designated by mean mixture fraction and mean jet fluid age coordinates. The

independent variation suggests that, for the wide variety of practical combustion systems involving fluid injection, the mean fluid age may provide a useful scalar marker field for describing the mixing between regions of fluid that may have the same mixture fraction, but which have different compositions on account of having been injected at different times.

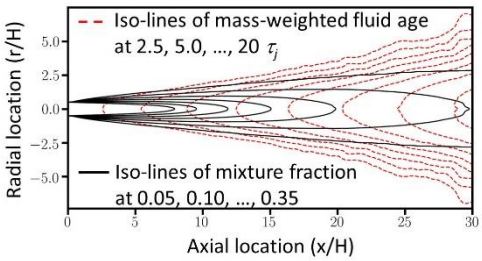

Figure 1. Iso-lines of mean mixture fraction (solid) and mass weighted jet fluid age (dashed) for a statistically-stationary round turbulent jet with jet Reynolds number of 7,290 [5].

The objective of this study is to investigate the relationship between the distribution of reactive scalars and the joint distribution of mixture fraction and fluid age within a turbulent lifted non-premixed jet flame. This relationship is investigated through statistical analysis of DNS data for a turbulent dimethyl-ether (DME) lifted jet flame [14]. In particular, the analysis uses the DNS data to evaluate the accuracy of a first-order double conditional moment closure for reaction rates, double-conditioned on mixture fraction and fluid age, given by

$$\left\langle \omega_i\left(\vec{x},t\right)\right\rangle = \iint\left[\omega_i\left(\left\langle \boldsymbol{Y}\,|\,\eta,\alpha;\vec{x},t\right\rangle\right)\times P\left(\eta,\alpha;\vec{x},t\right)\right]d\eta d\alpha\,, \tag{2}$$

where $\boldsymbol{Y}$ is the vector of species mass fractions, temperature and pressure, ω_i is the reaction rate for the i^{th} species, η and α are sample-space variables for mixture fraction and fluid age, $P\left(\eta,\alpha;\vec{x},t\right)$ is the joint probability density function (pdf) of mixture fraction and fluid age, $\left\langle\cdot\right\rangle$ denotes ensemble averaging, and $\left\langle\cdot\,|\,\eta,\alpha\right\rangle$ denotes conditional averaging on mixture fraction (η) and fluid age (α). Modelling for the joint pdf $P\left(\eta,\alpha;\vec{x},t\right)$ is also investigated through analysis of the DNS dataset.

2. Direct Numerical Simulation

The analysis considers data from direct numerical simulation of a lifted dimethyl ether turbulent jet flame, simulated by Minamoto and Chen [14]. A planar jet of diluted DME fuel issues into a coflow of air at hot, high pressure conditions at which the fuel-air mixture undergoes two-stage ignition – exhibiting both low temperature heat release and negative temperature coefficient (NTC) behaviour. The lifted flame is established by forced ignition of mixture that has undergone first-stage ignition, but at a location far upstream of where second-stage ignition would occur spontaneously. The lifted flame configuration is illustrated in Figure 2a by volume rendering of methoxymethyl-peroxy mass fraction ($Y_{CH3OCH2O2}$), a marker of low-temperature heat release, and hydroxyl radical mass fraction (Y_{OH}), an indicator of high-temperature heat release. The flow is periodic in the span-wise z-direction. Minamoto and Chen [14] characterise the leading points of the flame base predominantly as propagating deflagaration fronts with significant contributions from molecular diffusion, rather than as autoignition fronts. However, the flame propagation speed at the flame base appears to be enhanced significantly by the presence of the partially-reacted mixture produced by the first-stage ignition. Chemical activity is also significant in the mixture upstream of the flame base, with conditional statistics revealing bands of heat release consistent with the upstream branches of polybrachial flame structures observed in laminar flames at similar thermochemical conditions [15].

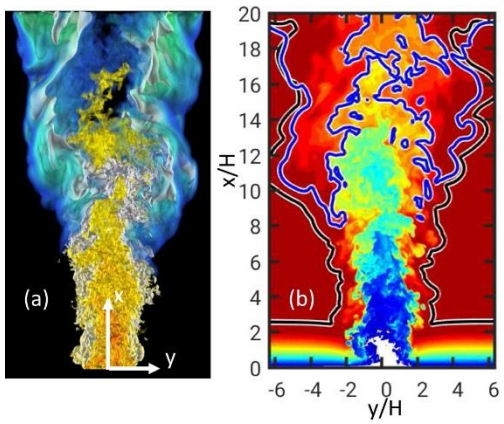

Figure 2. (a) Instantaneous volume rendering of the turbulent DME lifted jet flame showing the coordinate system and a low-temperature heat release marker, $Y_{CH3OCH2O2}$ (yellow-red colours) and a high-temperature flame marker, Y_{OH} (blue-green colours). (b) Contour line of a=97 τ_j (black) and contour line of Y_{OH}=0.2$Y_{OH,Max}$ (blue) overlaid on the normalized age variable field, a/τ_j, (colour) in the span-wise mid plane at t/τ_j=64 [1].

2.1 Simulation configuration

In order to achieve a DNS with a high-intensity of shear-generated turbulence at the flame base, the spatially-evolving turbulent jet flame is initialised from the solution of a separate temporally-evolving planar turbulent slot jet DNS, as described in Ref. [14]. The temporally-evolving simulation is itself initialised from a 5.4 *ms* duration laminar mixing layer simulation. First-stage ignition takes place during the laminar phase of the simulation, and a shear-generated turbulent velocity field develops during the 40 μs of the temporal jet simulation. The partially-reacted inflow conditions for the spatially-evolving jet simulation are obtained by scanning through a snap-shot of the temporally-evolving jet solution. The high-temperature flame is established by artificially increasing the temperature in a narrow downstream region of the domain in the initial condition of the spatially-evolving jet simulation.

The fuel and oxidiser streams are composed of 0.1DME+0.9N_2 and 0.21O_2+0.79N_2 by volume, giving a stoichiometric mixture fraction equal to ξ_{st}=0.42. The pressure is 5 atm, and the fuel and oxidiser temperatures are 500 K and 1000 K leading to two-step ignition and NTC behaviour. The initial width of the fuel jet in the laminar simulation is H=0.6 *mm*, and the initial fuel jet and coflow velocities in the temporal jet simulation are u_j=138 ms^{-1} and u_{cof}=3 ms^{-1}. At the inlet to the spatially-evolving DNS, the centreline stream-wise mean velocity has decayed to 104 ms^{-1} and shear-generated turbulence is established with a Taylor-scale Reynolds number of 79 based on the centreline stream-wise velocity fluctuations [14].

2.2 Numerical implementation

The flame is simulated using the Sandia DNS code S3D [16]. The code solves the fully-compressible conservation equations for mass, momentum, total energy and species mass fractions. Chemical reaction is described by a reduced mechanism for DME-air combustion involving 30 species [17]. Molecular transport is modelled using mixture-averaged transport coefficients and species specific-heats are modelled as polynomial functions of temperature. In addition, transport equations are solved for fluid age (Eq. (1)) and for mixture fraction (Eq. (3)),

$$\frac{\partial \xi}{\partial t} + \vec{u} \cdot \nabla \xi = \frac{1}{\rho} \nabla \cdot \left(\rho \mathscr{D} \nabla \xi \right). \tag{3}$$

The mixture fraction and fluid age are passive scalars used in the data analysis that do not affect the flow field. Differential diffusion does not have a leading-order effect on the lifted DME-flame analysed in this study, and the mixture fraction and fluid age diffusivities are set equal to the diffusivity of nitrogen since nitrogen accounts for 79-90% of the mixture by volume. The fluid age within the domain is initialised equal to zero at the start of the spatially-developing jet simulation and remains equal to zero at the inlet boundary for the duration of the simulation. Due to the slow co-flow velocity, the fluid age field does not reach a steady-state condition throughout the domain during the simulation.

The domain of the spatially-evolving jet DNS spans $L_x \times L_y \times L_z = 20H \times 20H \times 5H$ where *x*, *y* and *z* refer to the coordinate system shown in Figure 2a. The domain is discretised using 1512x896x384 grid points, with a uniformly-spaced 8 μm mesh across the cross-stream region containing the turbulent fuel jet. The solver uses 8th-order explicit finite differences [18], and characteristic boundary conditions [19,20].

After 215 μs (2.5 flow through times) the high-enthalpy fluid used to ignite the flame has left the domain, and a further 2.3 flow through times (205 μs) are simulated, during which time the flame base moves slowly downstream from *12H* to *14H*. Due to the high jet velocity, the fluid age statistics in the near-field of the jet rapidly approach a quasi-stationary state, which evolves slowly as the flame stabilisation point moves downstream. Due to the low coflow velocity, the coflow-fluid does not wash through the domain during the simulation time, as shown in Figure 2b, and the age field away from the jet is affected by the initialization of the age variable. The analysis of age-conditioned statistics is therefore restricted to the higher-mixture fraction regions within the jet where the age field is found to be quasi-stationary.

3. Results

The relationship between the joint mixture fraction/fluid age distribution and the reactive scalar distribution is assessed first by characterising the joint mixture fraction/fluid age distribution, and subsequently by evaluating the double-conditional averages appearing in Eq. (2) for key intermediate and product species.

3.1 The Mixture Fraction/Fluid Age Joint Distribution

Marginal pdfs for mixture fraction $P_{\xi}\left(\eta;\vec{x},t\right)$ and fuid age $P_a\left(\alpha;\vec{x},t\right)$ are presented in Figure 3 for a number of positions along the jet centreline at *x/H*=2,4,…,16 sampled from t/τ_j=90-97, where $\tau_j = H/u_j$. The pdfs presented in this section are averaged over the periodic *z*-direction and time-averaged over a period of $7\tau_j$ in order to obtain a greater statistical sample size from the DNS data, noting that $7\tau_j$ is still short compared to the time period over which the flame base is moving downstream (approximately *1H* in $20\tau_j$). The mean and variance of the fluid age distribution increase downstream, while the mean and variance of the mixture fraction decrease downstream. However the pdf shapes shown in Figure 3b,d, for the standardised variables $\left(\eta - \overline{\xi}\right)/\xi'$ and $\left(\alpha - \overline{a}\right)/a'$ are uniform along the jet axis. Standardisation is achieved by subtracting the mean, $\overline{a}$ and $\overline{\xi}$, and dividing by the root-mean-square value, ξ' and a'. The observation that the standardised mixture fraction and fluid age pdfs are uniform along the axis is

consistent with previous observations that the jet fluid age and mixture fraction both exhibit self-similar behaviour in fully-developed turbulent jets [5].

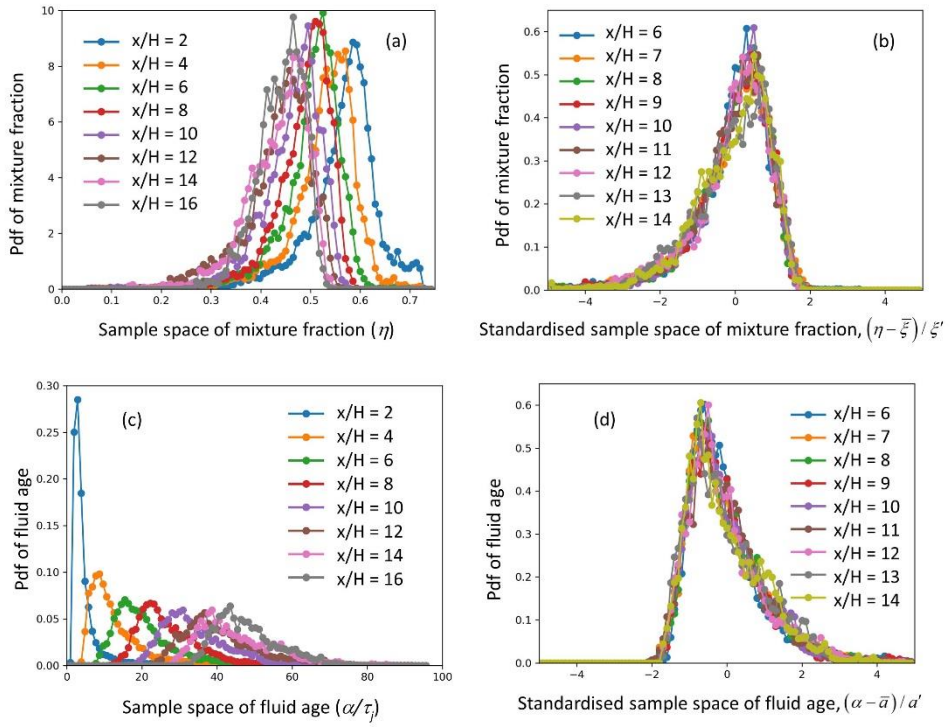

Figure 3. Probability density functions for mixture fraction (a) and fluid age (c) on the jet centreline at x/H=2,…,16 sampled over t/τ_j=90-97. (b) and (d) show the standardised pdfs corresponding to (a) and (c).

The centreline pdfs of standardised mixture fraction and fluid age have similarly skewed shapes, but with opposite skewness. Figure 4 presents the pdfs for $(\eta-\bar{\xi})/\xi'$ and $-(\alpha-\bar{a})/a'$ along $y=0.035(x-x_0)$, with the virtual origin x_0 =1.4H. The marginal pdfs in Figure 4 may be approximated by the β-function distribution [21] or, more accurately, by the skewed-normal distribution. While the three parameter skewed-normal distribution gives slightly closer agreement to the observed pdf shapes, the β-function distribution is used widely to model the mixture fraction distribution in presumed-pdf turbulent combustion modelling as it ensures boundedness and requires modelling for only two input parameters. The skewed-normal distribution in contrast is not realisable for all values of skewness observed in the DNS. The similarity between the marginal pdf shapes for the standardised mixture fraction and fluid age suggests that the β-function distribution may also be used to provide a similar fidelity of modelling for the fluid age distribution.

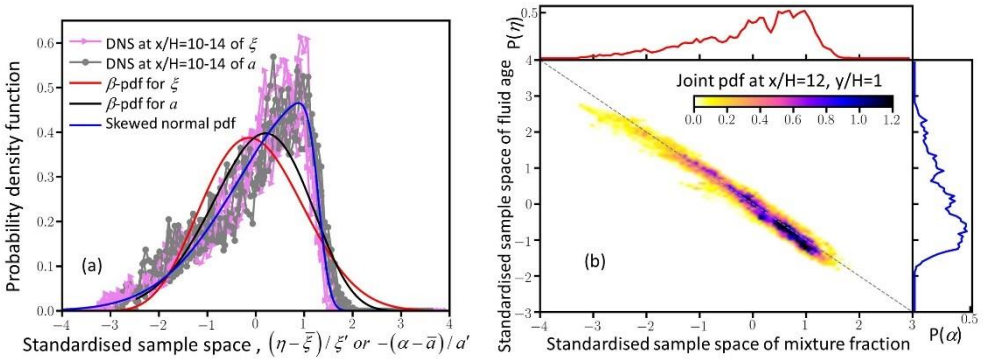

Figure 4. Standardised (a) marginal- and (b) joint-pdfs of mixture fraction and fluid age sampled over t/τ_j=90-97, with presumed pdf shapes given by the β-function and skewed-normal distributions. Marginal distributions are for x/H=6,…,14 and y=0.035(x-x_0), and the joint distribution is for x=12H, y=H.

The joint pdfs of mixture fraction and fluid age in Figure 5 show strong negative correlation between the mixture fraction and fluid age throughout the jet. The deviations from the line $(\alpha-\bar{a})/a' = -(\eta-\bar{\xi})/\xi'$ are small. Assumption that these deviations follow a normal distribution with standard deviation σ, and that the mixture fraction marginal pdf can be modelled adequately, leads to a simple model for the joint distribution of mixture fractions and fluid age:

$$P_{\xi a}(\eta,\alpha) = \frac{P_{\xi}(\eta)}{a'\sqrt{2\pi\sigma^2}} \times \exp\left(-\frac{1}{2\sigma^2}\left[\left(\frac{\alpha-\bar{a}}{a'}\right) + \left(\frac{\eta-\bar{\xi}}{\xi'}\right) \right]^2 \right) . \tag{4}$$

In the limit of a small standard deviation, $\sigma \to 0$, the joint distribution can be further simplified as:

$$P_{\xi a}(\eta,\alpha) = P_{\xi}(\eta) \cdot \delta\left(\left(\frac{\alpha-\bar{a}}{a'}\right) + \left(\frac{\eta-\bar{\xi}}{\xi'}\right) \right) , \tag{5}$$

where δ(.) is the Dirac delta function.

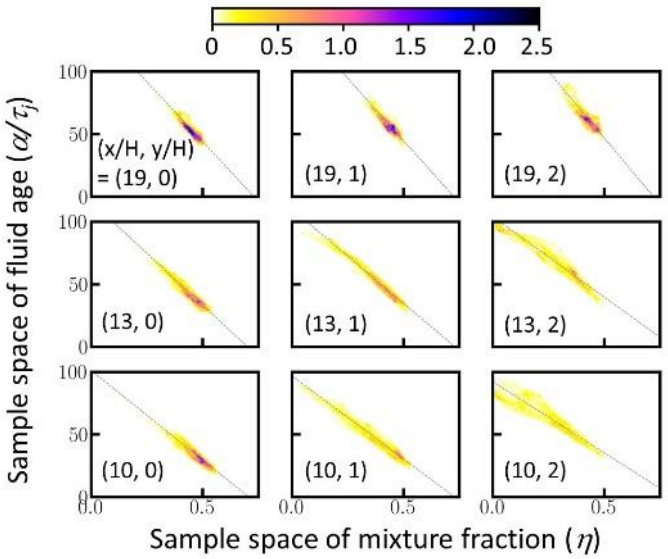

Figure 5. Joint probability density function of mixture fraction and fluid age at a number of stream-wise and span-wise positions, designated by values for (*x*/*H*, *y*/*H*), sampled over t/τ_j=90-97. The dashed line plots the locus of $(\alpha-\bar{a})/a' = -(\eta-\bar{\xi})/\xi'$.

The joint mixture fraction/fluid age pdf predicted by Eq. (4) with σ=0.25 is compared with the empirical joint pdf sampled from the DNS in Figure 6. Predictions are shown using either the empirical marginal pdf for mixture fraction obtained from the DNS, or using the β–function to presume the marginal pdf for mixture fraction. The joint pdf predicted by Eq. (5) (not shown) is the projection of the pdf given by Eq (4) onto the line $(\alpha-\bar{a})/a' = -(\eta-\bar{\xi})/\xi'$. The comparison shows that Eq. (4) gives good predictions for the joint mixture fraction/fluid age distribution within the jet when the marginal pdf of mixture fraction is modelled accurately. The β-function distribution under-predicts the skewness of the mixture fraction distribution and therefore also of the fluid age distribution, however the level of accuracy given by the β-function is often accepted for the purposes of presumed pdf modelling in non-premixed combustion.

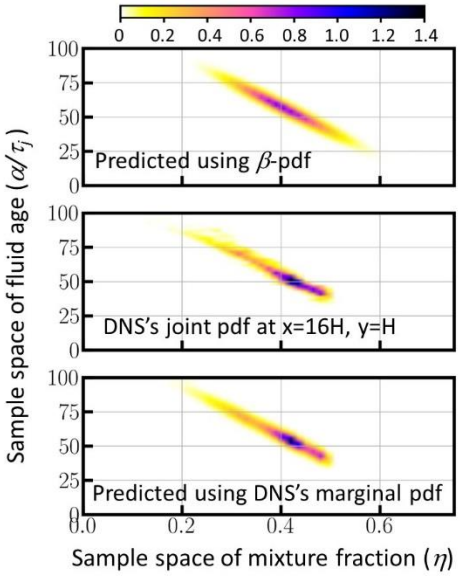

Figure 6. Joint probability density function of mixture fraction and fluid age at *x=16H*, *y=H*, sampled over t/τ_j=90-97.

3.2 Reactive Scalar Distributions

Figure 7 presents the joint distribution of CO_2 mass fraction and mixture fraction at t/τ_j=96, conditioned on two values of fluid age, a/τ_j=82 and 95. Although the data are sampled from the whole domain, the distribution shows that the CO_2 mass fraction is distributed narrowly around a two-dimensional manifold in mixture fraction/fluid age space. This observation implies that the mixture fraction/fluid age coordinates resolve the overall variation of the mean progress variable throughout the domain. The fact that the mixture fraction/fluid age space provides a useful mapping for major reactant species like CO_2 can be understood by referring to Figure 1, which showed that the mean mixture fraction

and mean fluid age form a coordinate system in the fully-developed jet that maps uniquely to the stream-wise/cross-stream spatial coordinates of the jet, and therefore to the mean progress variable field of a statistically-symmetrical lifted jet flame. The spatial homogeneity of the mixture fraction/fluid age–conditioned statistics of reactive scalars in the present flow simplifies modelling since it might not be essential to account for spatial variation of the conditional averages even if, more generally, spatial inhomogeneity can be taken into account using conditional moment transport equations [22].

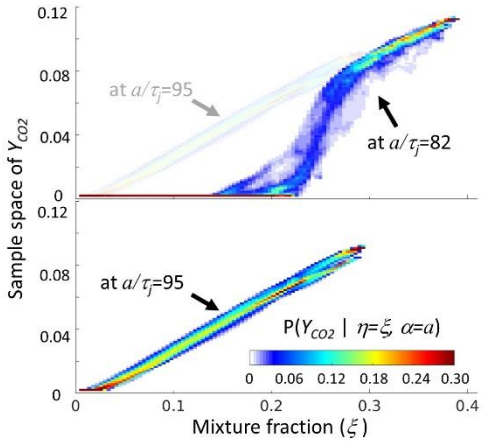

Figure 7. False colour of pdf of Y_{CO2} conditioned on mixture fraction and age, $P\left(Y_{CO2} \mid \eta = \xi, \alpha = a\right)$ for a/τ_j=82 (top) and a/τ_j=95 (bottom and top in faint colour).

The first order double conditional moment closure, conditional on mixture fraction and fluid age is tested by integrating Eq. (2) with the pdf given either by Eq. (4) with σ=0.25 or by Eq. (5). The value of σ=0.25 is chosen as it describes the width of the joint distribution well throughout the domain. This *a priori* analysis uses the double-conditioned average composition from the whole domain at t/τ_j=90-97. The one point joint pdfs of mixture fraction and fluid age are obtained by (*i*) direct sampling from the DNS, (*ii*) Eq. (4) using the marginal pdf for mixture fraction from the DNS, or (*iii*) Eq. (4) using the β–function presumed pdf for mixture fraction. Predictions of the unconditional reaction rates are presented in Figure 8 for CO_2, an example of a major product species, and for H_2O_2, which is formed by the pre-ignition chemical processes occurring after first stage ignition and before reaching the flame base. Except very close to the inlet, where the fluid age profile is still developing, the presumed-pdf model for the joint mixture fraction/fluid age distribution based on use of the β–function in Eq. (4) provides predictions for the unconditional reaction rates in close agreement with predictions based on the joint-pdf sampled from the DNS. The relatively small difference between the predictions given by Eqs. (4) and (5) indicates that there is a low sensitivity to value of σ. Given the similar results, Eq. (5) may be preferred for computational reasons, since the integration of Eq. (2) becomes a one-dimensional integration along the line $\left(\alpha - \overline{a}\right)/a' = -\left(\eta - \overline{\xi}\right)/\xi'$. We note that success in *a priori* testing is neither necessary nor sufficient reason to conclude that an approach will provide accurate predictions in *a posteriori* simulations. However, it is encouraging that the agreement given by the first-order double conditional moment closure is generally satisfactory throughout the domain, both for intermediate species that characterise the progress of ignition processes upstream of the flame base, and for major species that undergo their greatest changes within the high temperature flame.

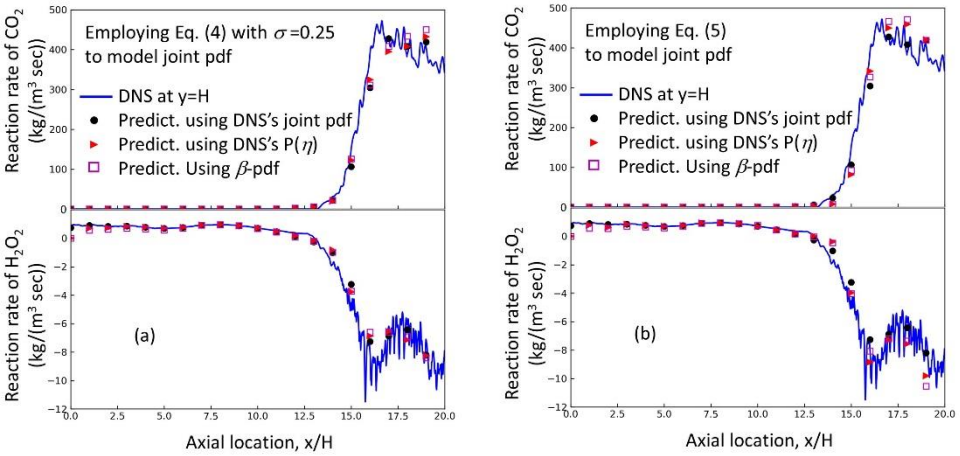

Figure 8. Comparison of the unconditional mean reaction rate for CO_2 (top) and H_2O_2 (bottom) mass fractions along the stream-wise direction offset from the centreline at $y=H$, t/τ_j=90-97, using either (a) Eq. (4) or (b) Eq. (5) to model the joint pdf.

4. Conclusion

Direct numerical simulation analysis of a lifted DME turbulent jet flame shows that the distribution of the reactive scalars is related to the joint distribution of mixture fraction and fluid age. The fluid age transport equation provides a local measure of the average residence time within the flow; it exhibits self-similar profiles in fully-developed turbulent jets that are distinct from mixture fraction profiles; and, in combination with the mixture fraction, it serves as a useful mapping variable to distinguish younger less-reacted fluid near the inlet from older more-reacted fluid downstream. The local fluctuations of mixture fraction and fluid age have strong negative correlation and, building upon established presumed-pdf models for mixture fraction, this feature can be used to construct an accurate presumed-pdf model for the joint mixture fraction/fluid age pdf. Information about the joint distribution can be useful in a variety of settings: In this study, it is demonstrated that the double-conditional first-order moment closure gives accurate predictions for unconditional reaction rates – both for pre-ignition radical species produced by low-temperature processes upstream of the flame base, and for major species that are produced at the flame front. Furthermore, low values of fluid age at the flame base (approximately one order of magnitude shorter than the second stage ignition delay time [14]) indicate that this DNS flame is stabilised predominantly by propagation through a mixture that has undergone first-stage ignition. The fluid age therefore provides information about the extent of ignition progress upstream of the flame base that should be used as a guide to selection of combustion models that account for the prevailing flame stabilisation mechanism and, where applicable, should be taken into account in modelling the flame propagation speeds [23].

5. Acknowledgements

Sandia National Laboratories is a multimission laboratory managed and operated by National Technology & Engineering Solutions of Sandia, LLC, a wholly owned subsidiary of Honeywell International Inc., for the U.S. Department of Energy's National Nuclear Security Administration under contract DE-NA0003525. The views expressed in the article do not necessarily represent the views of the U.S.

Department of Energy or the United States Government. Shin, Richardson and Aparace-Scutariu are grateful for support from the Engineering and Physical Science Research Council (UK) under grants EP/L002698/1, EP/K024876/1, EP/M001482/1, and EP/N509644/1.

6. References

[1] L. Gomet, V. Robin, and A. Mura, Combust. Sci. Technol. 184 (10-11) (2012) 1471–1501.
[2] N. Enjalbert, P. Domingo, and L. Vervisch, Combust. Flame 159 (1) (2012) 336–352.
[3] S. Batterman, Assessment of Small-Scale Incinerators for Health Care Waste, Tech. Rep., World Health Organization, 2004.
[4] R. W. Grout, Phys. Fluids 19 (10) (2007) 105–107.
[5] D. Shin, R. D. Sandberg, and E. S. Richardson, J. Fluid Mech. 823 (2017) 1–25.
[6] I. Langmuir, J. Am. Chem. Soc. 30 (11) (1908) 1742–1754.
[7] P. V. Danckwerts, Chem. Eng. Sci. 2 (1) (1953) 1–13.
[8] D.B. Spalding, Chem. Eng. Sci. 9 (1) (1958) 74 –77.
[9] E. Mastorakos, T. A. Baritaud, and T. J. Poinsot, Combust. Flame 109 (1-2) (1997) 198–223.
[10] R. W. Bilger, S. Kim, and S. Martin, Direct numerical simulation of turbulent premixed flames with a marker field and application to RANS and LES, Proceedings of the Summer Program (2004), Center for Turbulence Research. Stanford, CA, 2004, 255–267.
[11] M. Sandberg, Build. Environ. 16 (2) (1981) 123–135.
[12] F. Ghirelli and B. Leckner, Chem. Eng. Sci. 59 (3) (2004) 513–523.
[13] D. Shin, A. J. Aspden, and E. Richardson, International Symposium on Turbulent Shear Flow Phenomena, Chicago, USA, July, 2017.
[14] Y. Minamoto and J. H. Chen, Combust. Flame 169 (2016) 38–50.
[15] A. Krisman, E. R. Hawkes, M. Talei, A. Bhagatwala, and J. H. Chen, Proc. Combust. Inst. 35 (1) (2015) 999–1006.
[16] J. H. Chen, A. Choudhary, B. De Supinski, M. DeVries, E. R. Hawkes, S. Klasky, W. Liao, K. Ma, J. Mellor-Crummey and N. Podhorszki, Comp. Sci. Discov. 2 (1) (2009) 015001.
[17] A. Bhagatwala, R. Sankaran, S. Kokjohn, and J. H. Chen, Combust. Flame 162 (9) (2015) 3412–3426.
[18] C. A. Kennedy and M. H Carpenter, Appl. Numer. Math. 14 (4) (1994) 397–433.
[19] T. J. Poinsot and S.K. Lele, J. Comp. Phys. 101 (1) (1992) 104–129.
[20] J. C. Sutherland and C. A. Kennedy, J. Comp. Phys. 191 (2) (2003) 502–524.
[21] C. S. Yoo, R. Sankaran, and J. H. Chen, J. Fluid Mech., 640, (2009) 453-481.
[22] A. Klimenko and R. W. Bilger, Prog. Energ. Combust. 25 (6) (1999) 595–687.
[23] B. S. Soriano, E. S. Richardson, S. Schlatter, and Y. M. Wright. SAE (2017), Powertrains, Fuels and Lubricants, Beijing, China, 2017.